Electronic Supplementary Information

$Pb_6Ba_3Si_2S_8I_{10}$: A new thiohalide with a quasi-two-dimensional structure and wide band gap

Wang Zhao,[a,b] Jiazheng Zhou,[a] Linan Wang,[a,b] Wenqi Jin,[a,b] Yingying Kong,[a] Yu Chu[a,b*] and Junjie Li[a,b*]

[a]*Research Center for Crystal Materials; CAS Key Laboratory of Functional Materials and Devices for Special Environments, Xinjiang Technical Institute of Physics & Chemistry, CAS, Urumqi 830011, China*

[b]*Center of Materials Science and Optoelectronics Engineering, University of Chinese Academy of Sciences, Beijing 100049, China*

*Corresponding author: chuy@ms.xjb.ac.cn (Yu Chu), lijunjie@ms.xjb.ac.cn (Junjie Li)

CONTEXT

Table S1 Atomic coordinates (× 10^4), equivalent isotropic displacement parameters (Å^2 × 10^3) and bond valence calculations (BVSs) for $Pb_6Ba_3Si_2S_8I_{10}$.

Table S2 Bond lengths [Å] and angles [deg] for $Pb_6Ba_3Si_2S_8I_{10}$.

Table S3 Crystal systems, space groups, experimental band gaps and structural dimensions of known AM- and/or AEM-contained Pb-based thiohalides without C, H, O, N elements in ICSD.

Figure S1 The EDS spectrum and mappings of $Pb_6Ba_3Si_2S_8I_{10}$.

Figure S2 The distribution of Ba cations and I ions in the quasi-2D layers of $Pb_6Ba_3Si_2S_8I_{10}$.

Figure S3 The IR absorption spectrum of $Pb_6Ba_3Si_2S_8I_{10}$.

Figure S4 The Rietveld refinements of $Pb_6Ba_3Si_2S_8I_{10}$ based on the powder XRD pattern.

Figure S5 XRD patterns of $Pb_6Ba_3Si_2S_8I_{10}$ before and after heating at 1130 K.

Figure S6 Diffuse reflectance spectrum of $Pb_6Ba_3Si_2S_8I_{10}$ plotted as $[(kvF(R)]^{1/2}$ (indirect band gap), where $F(R)$ is the Kubelka−Munk function. Dotted lines show the fit used to extract the band gap.

Figure S7 The RID measurement result of $Pb_6Ba_3Si_2S_8I_{10}$.

Table S1 Atomic coordinates (× 10^4), equivalent isotropic displacement parameters (Å^2 × 10^3) and bond valence calculations (BVSs) for $Pb_6Ba_3Si_2S_8I_{10}$.

Atom	Wyckoff	*x*	*y*	*z*	U(eq)	BVS[a]
Ba(1)	18*e*	3333.33	3221.0(10)	4166.67	45.8(3)	2.31
Pb(1)	36*f*	3447.7(6)	791.3(6)	4756.2(2)	43.02(17)	1.83
Si(1)	12*c*	6666.67	3333.33	4474.7(6)	15.8(8)	3.94
S(1)	12*c*	6666.67	3333.33	4779.4(5)	16.4(7)	2.12
S(2)	36*f*	4603(3)	1297(3)	4381.9(3)	20.3(5)	2.15
I(1)	36*f*	3267.0(8)	4112.2(9)	4749.3(2)	33.8(2)	0.95
I(2)	6*b*	0	0	5000	19.1(3)	0.79
I(3)	6*a*	3333.33	6666.67	4166.67	78.0(10)	0.80
I(4)	12*c*	0	0	4436.8(2)	37.9(3)	0.79
		GII[b]			0.178	

[a] The bond valence sum is calculated by bond-valence theory (S_{ij} = exp[(R_0-R)/B, where R is an empirical constant, R_0 is the length of bond I (in angstroms), and B = 0.37).

[b] The global instability index (GII) calculated using:

$$G = \sqrt{\frac{\sum_{i=1}^{n}(BVS - v_i)}{N}}$$

where N is the number of atoms in the formula unit. The GII is calculated as 0.178 which is lower than 0.2 indicating the rationality of the structure from this side.

Table S2 Bond lengths [Å] and angles [deg] for $Pb_6Ba_3Si_2S_8I_{10}$.

Pb(1)-I(1)	3.3443(9)	S(2)#2-Ba(1)-I(4)#3	81.45(4)
Pb(1)-I(2)	3.5138(5)	I(2)-Ba(1)-I(4)	114.051(15)
Ba(1)-S(2)	3.122(2)	I(2)-Ba(1)-I(4)#4	114.051(15)
Ba(1)-S(2)#1	3.122(3)	S(2)#5-Si(1)-S(1)	108.09(12)
Ba(1)-S(2)#2	3.266(2)	S(2)#2-Si(1)-S(1)	108.09(12)
Ba(1)-S(2)#3	3.266(2)	S(2)-Si(1)-S(1)	108.08(12)
Ba(1)-I(4)	3.7346(7)	S(2)-Si(1)-S(2)#5	110.82(12)
Ba(1)-I(4)#4	3.7345(7)	S(2)#5-Si(1)-S(2)	110.82(12)
Ba(1)-I(3)	3.3742(10)	S(2)-Si(1)-S(2)#2	110.82(12)
Si(1)-S(1)	2.152(5)	I(1)-Pb(1)-I(2)	73.110(16)
Pb(1)#5-S(1)	2.8832(6)	S(1)-Pb(1)-I(2)	132.67(5)
Pb(1)-S(1)	2.8832(6)	S(1)-Pb(1)-I(1)	74.207(17)
Pb(1)#3-S(1)	2.8832(6)	S(2)-Pb(1)-I(2)	139.01(5)
Si(1)-S(2)	2.112(3)	S(2)-Pb(1)-I(1)	91.56(5)
Pb(1)-S(2)	2.821(2)	S(2)-Pb(1)-S(1)	74.47(8)
S(2)#1-Ba(1)-S(2)	73.24(9)	S(2)#1-Ba(1)-I(4)	70.15(5)
S(2)-Ba(1)-S(2)#2	65.92(8)	S(2)#1-Ba(1)-I(3)	81.45(4)
S(2)#1-Ba(1)-S(2)#2	130.29(3)	S(2)-Ba(1)-I(3)	143.38(4)
S(2)#1-Ba(1)-S(2)#3	130.29(3)	S(2)#2-Ba(1)-I(3)	143.38(4)
S(2)#1-Ba(1)-S(2)#3	65.92(8)	S(2)-Ba(1)-I(4)#4	70.16(5)
S(2)#2-Ba(1)-S(2)#3	162.89(9)	S(2)#3-Ba(1)-I(4)	68.76(4)
S(2)#2-Ba(1)-I(4)	118.91(4)	S(2)#1-Ba(1)-I(4)#4	71.66(5)
S(2)#2-Ba(1)-I(4)#4	68.76(4)	S(2)#3-Ba(1)-I(4)#4	118.91(4)
S(2)-Ba(1)-I(4)	71.65(5)		

Symmetry transformations used to generate equivalent atoms:

#1 2/3-x,1/3-x+y,5/6-z #2 1+y-x,1-x,+z #3 -1/3-y+x,1/3-y,5/6-z

#4 2/3+y,1/3+x,5/6-z #5 1-y,+x-y,+z #6 -y,+x-y,+z #7 +y-x,-x,+z

#8 1-y,1+x-y,+z #9 +y-x,1-x,+z

Table S3 Crystal systems, space groups, experimental band gaps and structural dimensions of known AM- and/or AEM-contained Pb-based thiohalides without C, H, O, N elements in ICSD.

Compounds	Crystal system, space group	E_g (eV)	Structural dimension	Ref.
$Pb_5Sn_3Se_{10}Cl_2$	orthorhombic, *Cmmm*	1.44	3D	[1]
$Pb_5Sn_3S_{10}Cl_2$	orthorhombic, *Cmmm*	1.72	3D	[1]
$Pb_3Se_2Br_2$	cubic, $I\bar{4}3d$	1.48	3D	[2]
$Pb_5S_2I_6$	monoclinic, $C2/m$	1.73	3D	[3]
$Pb_4S_3I_2$	orthorhombic, *Pnma*	1.76	3D	[4]
$Pb_4S_3Br_2$	orthorhombic, *Pnma*	1.91	3D	[4]
$Pb_3S_3Cl_2$	cubic, $I\bar{4}3d$	2.02	3D	[4]
Pb_3SBrI_3	monoclinic, $P2_1/m$	2.16	3D	[5]
$Pb_2SbS_2I_3$	orthorhombic, *Cmmm*	2.19	3D	[6]
$[K_2PbI][Ga_7S_{12}]$	orthorhombic, *Imm*2	2.41	3D	[7]
$[K_2PbBr][Ga_7S_{12}]$	orthorhombic, Imm2	2.49	3D	[7]
$[K_2PbCl][Ga_7S_{12}]$	orthorhombic, *Imm*2	2.54	3D	[7]
$[Na_2PbI][Ga_7S_{12}]$	orthorhombic, *Imm*2	2.53	3D	[8]
$Pb_{3.5}GeS_4Br_3$	hexagonal, $P6_3$	2.6	3D	[9]
Pb_4SeBr_6	orthorhombic, *Imm*2	2.62	3D	[10]
$Pb_6Ba_3Si_2S_8I_{10}$	trigonal, $R\bar{3}c$	2.80	2D	This work

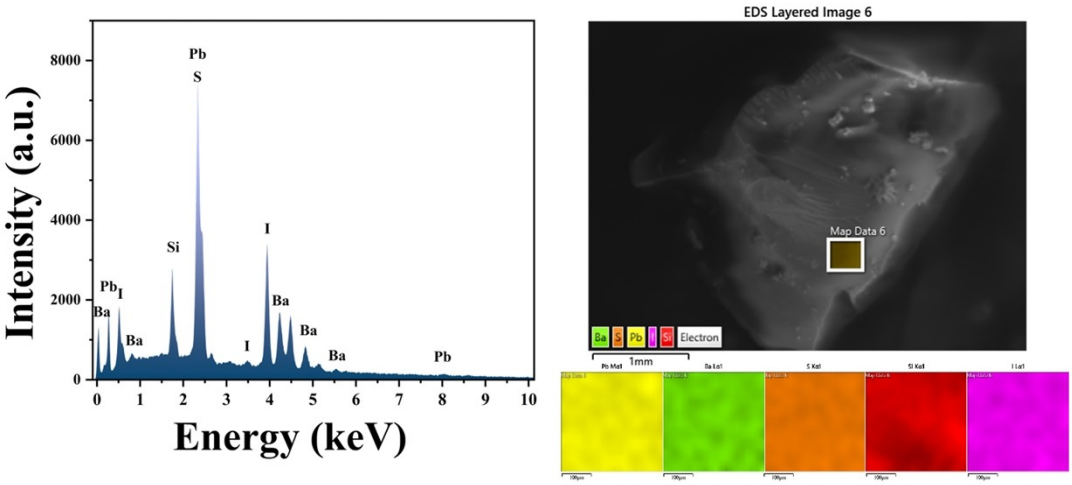

Figure S1 The EDS spectrum and mappings of $Pb_6Ba_3Si_2S_8I_{10}$.

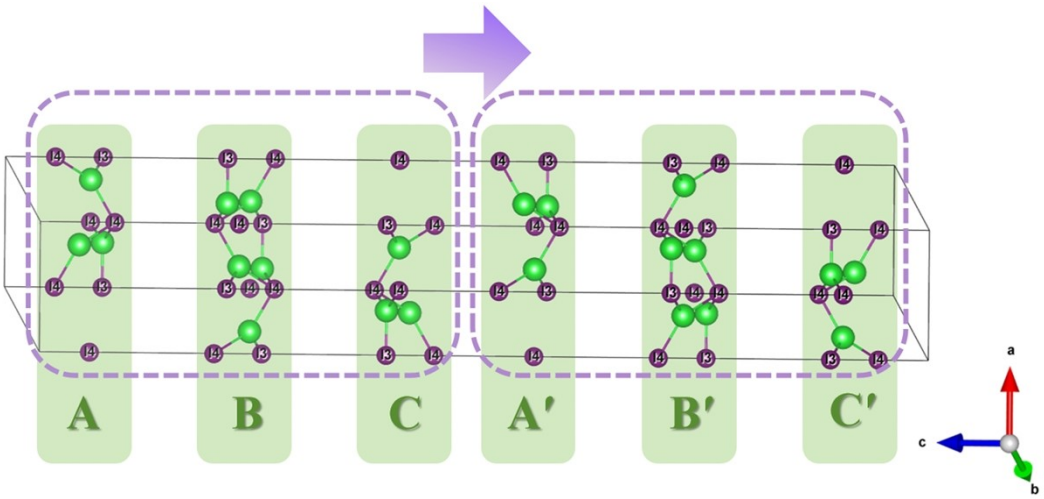

Figure S2 The distribution of Ba and I atoms in the quasi-2D layers of $Pb_6Ba_3Si_2S_8I_{10}$.

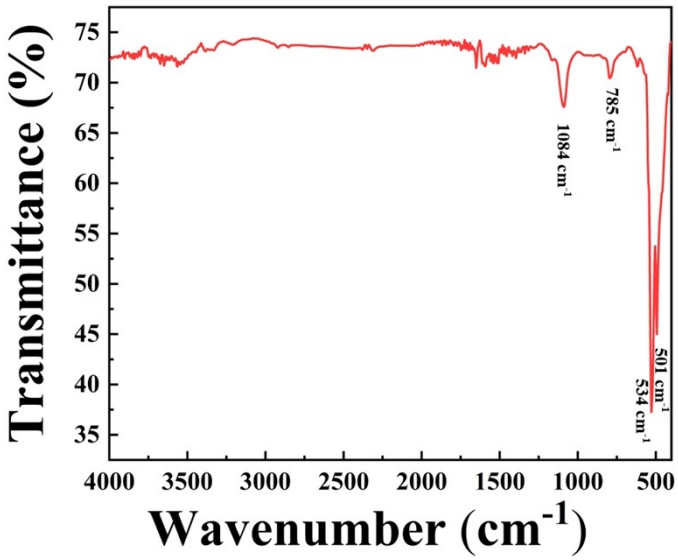

Figure S3 The IR absorption spectrum of $Pb_6Ba_3Si_2S_8I_{10}$.

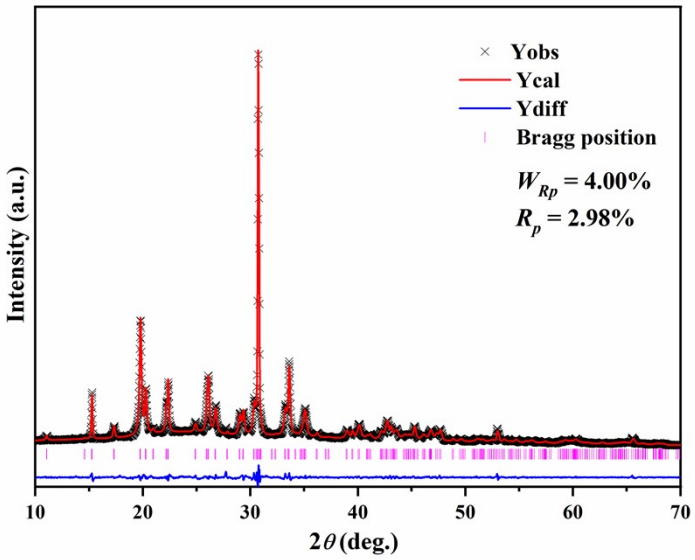

Figure S4 The Rietveld refinements of $Pb_6Ba_3Si_2S_8I_{10}$ based on the powder XRD pattern.

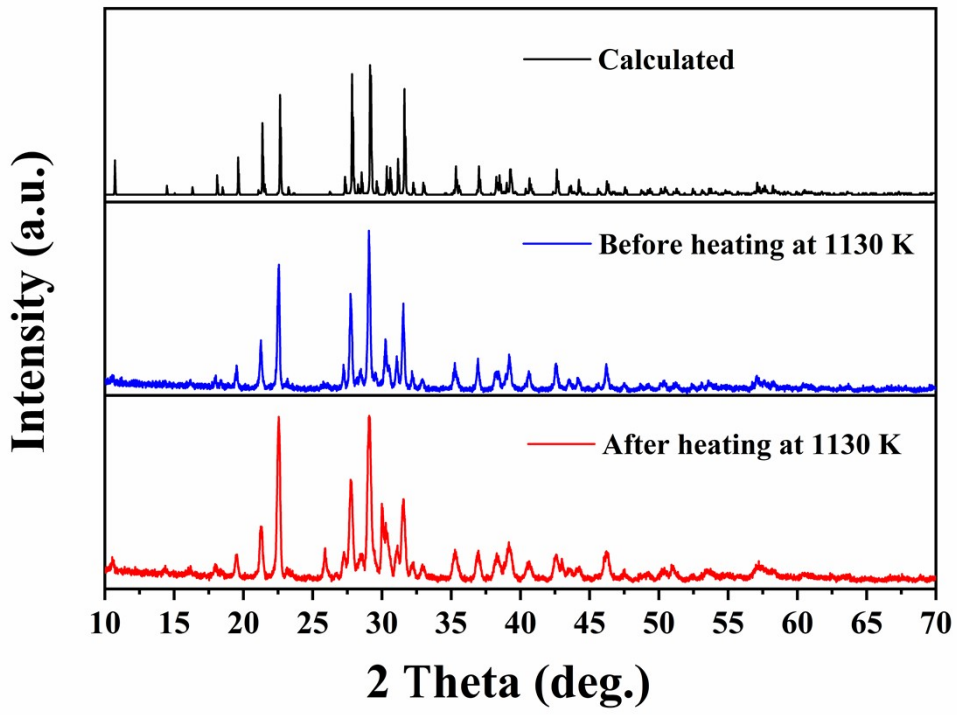

Figure S5 XRD patterns of $Pb_6Ba_3Si_2S_8I_{10}$ before and after heating at 1130 K.

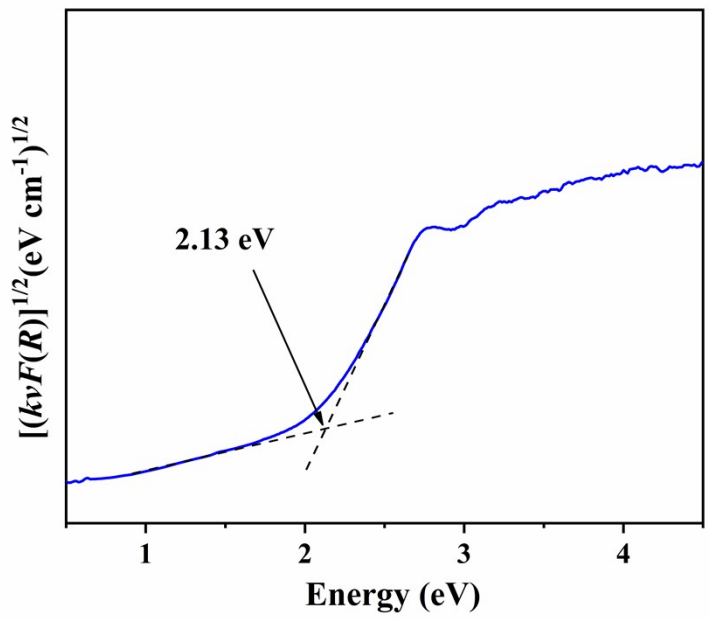

Figure S6 Diffuse reflectance spectrum of $Pb_6Ba_3Si_2S_8I_{10}$ plotted as $[(kvF(R)]^{1/2}$ (indirect band gap), where $F(R)$ is the Kubelka-Munk function. Dotted lines show the fit used to extract the band gap.

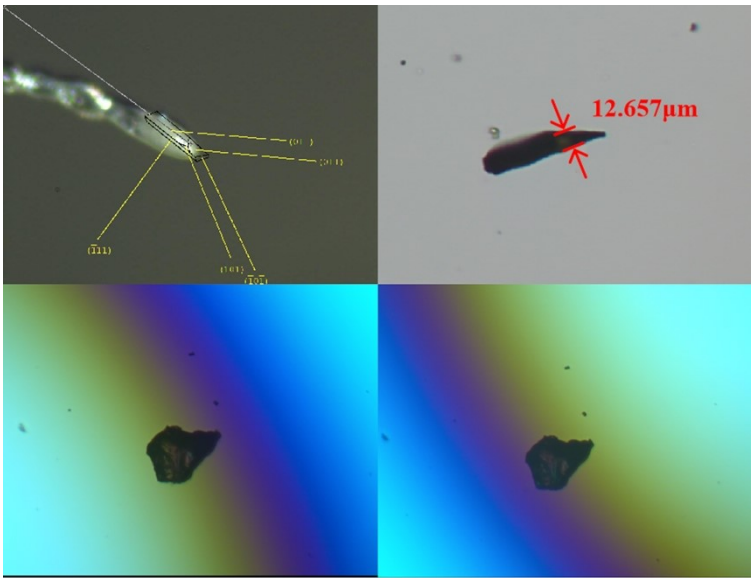

Figure S7 The RID measurement result of $Pb_6Ba_3Si_2S_8I_{10}$.

References

[1] L.-T. Jiang, M.-Z. Li, X.-M. Jiang, B.-W. Liu and G.-C. Guo, *Dalton Trans*., 2022, **51**, 6638-6645.

[2] D. Ni, S. Guo, K. M. Powderly, R. Zhong and R. J. Cava, *J. Solid State Chem*., 2019, **280**, 120982.

[3] H. Wang, G. Chen, J. Xu, Y. Xu and Q. Yang, *Cryst. Growth Des*., 2018, **18**, 1987-1994.

[4] S. Toso, Q. A. Akkerman, B. Martín-García, M. Prato, J. Zito, I. Infante, Z. Dang, A. Moliterni, C. Giannini, E. Bladt, I. Lobato, J. Ramade, S. Bals, J. Buha, D. Spirito, E. Mugnaioli, M. Gemmi and L. Manna, *J. Am. Chem. Soc*., 2020, **142**, 10198–10211.

[5] M. Yan, R.-L. Tang, W. Zhou, W. Liu and S.-P. Guo, *Dalton Trans*., 2022, **51**, 12921-12927.

[6] R. Nie, B. Kim, S.-T. Hong and S. I. Seok, *ACS Energy Lett*., 2018, **3**, 2376-2382.

[7] W.-F. Chen, B.-W. Liu, S.-M. Pei, X.-M. Jiang and G.-C. Guo, *Adv. Sci*., 2023, **10**, 2207630.

[8] Z.-X. Wu, W.-F. Chen, X.-M. Jiang, B.-W. Liu and G.-C. Guo, *Chem. Mater.*, 2024, **36**, 3444-3451.

[9] J. Zhou, H. Wang, J. Liu, X. Su, Y. Chu, J. Qu and X. Jiang, *Inorg. Chem. Front*., 2024, **11**, 2681-2689.

[10] J. Wang, H. Wu, H. Yu, Z. Hu, J. Wang and Y. Wu, *Adv. Opt. Mater*., 2022, **10**, 2102673.